Hindawi Publishing Corporation
International Journal of Antennas and Propagation
Volume 2007, Article ID 97481, 10 pages
doi:10.1155/2007/97481

Research Article

Analyses of a Dipole Antenna Loaded by a Cylindrical Shell of Double Negative (DNG) Metamaterial

Khan M. Z. Shams and Mohammod Ali

Received 1 December 2006; Accepted 3 August 2007

Recommended by Karu Esselle

The current distribution, input impedance, and radiation pattern of a cylindrical dipole antenna enclosed by a thin cylindrical shell of double negative (DNG) metamaterial are computed using the piecewise sinusoidal Galerkin formulation. In the presence of the DNG shell, the dipole antenna exhibits three interesting characteristics. The input impedance shows potentials for wide bandwidth due to the relative insensitivity of the impedance with frequency. Within specific ranges of DNG material parameter values, the dipole shows resonance at much lower frequencies than its resonant frequency in free space. The dipole does not show change in the direction of the principal beam nor does it show signs of beam splitting and side lobes even when the antenna length approaches one and a half wavelength.

1. INTRODUCTION

In 1968, Veselago first proposed theoretically that materials with simultaneously negative permittivity (ε_r) and permeability (μ_r) are permissible [1]. However, practical implementation of such a concept was not realized until the more recent developments described in [2–9]. Lately considerable interest has been shown on left-handed materials (LHM) due to their exciting performance characteristics in terms of focusing electromagnetic waves [10–13], microwave circuit miniaturization [14–16], and antenna performance improvement [17–22]. The authors of [17] have shown that the directivity of a circular patch antenna increases in the presence of a DNG material. In [19], Ziolkowski and Kipple presented a study of an infinitesimal dipole antenna (one five hundredth of a wavelength) surrounded by a spherical shell of DNG material. Their analytical and numerical results showed significant improvements in the radiation efficiency and the quality factor of the antenna. Ziolkowski also studied the matching of an electrically small antenna loaded with a spherical DNG shell [21]. Recently, we presented a preliminary analysis of the input impedance of a finite length wire dipole antenna loaded with a cylindrical shell of DNG material [22]. This work is a more detailed presentation of the abstract described in [22].

In this paper, we focus on examining the characteristics of a wire dipole antenna loaded with a cylindrical shell of DNG material using the piecewise sinusoidal Galerkin formulation. The primary objective of this investigation was to explore the possibilities of designing and developing broadband antennas and electrically small antennas using DNG loading. Questions that naturally arise are: (1) what are the differences in antenna current distribution between the conventional double positive (DPS) and DNG media?, (2) how do the antenna input impedance vary as function of frequency?, (3) is the input impedance of an electrically small dipole larger in a DNG medium than in a DPS medium, and (4) how does a DNG medium affect the radiation properties of the dipole antenna?

We study the current distribution, input impedance, VSWR bandwidth and radiation patterns of a cylindrical dipole loaded with a cylindrical shell of DNG material using the Galerkin method of moments (MoM) as described in [23]. For simplicity, in this work the cylindrical DNG shell surrounding the dipole antenna is considered homogeneous and isotropic. Variation of permittivity and permeability with frequency is also not considered.

The paper is organized as follows. Firstly, the MoM formulation used in this work is described followed by a validation of the formulation. Secondly, a discussion on the effects of the parameters P and Q (which are functions of the relative permittivity and permeability of the loading medium) on the antenna performance is given. Finally, a study of the antenna impedance, VSWR, and radiation characteristics as function of the DNG medium property is performed.

2. MOMENT METHOD FORMULATION

The geometry of the antenna and its surroundings are illustrated in Figure 1. The cross-sectional view of the antenna surrounded by a DNG medium is shown in Figure 1(b). In the MoM formulation, the integrations over the flat end surfaces of the wire antenna are neglected. The circumferential surface current component is also not considered. The skin depth is considered to be smaller than the wire radius in the frequency range of interest. Thus the current is confined to the antenna surface and the fields inside the antenna are virtually zero.

For a bare wire dipole, each piecewise sinusoidal function spans over two connected segments to form one element. Each element has a common segment which is shared with an adjacent element and hence can be considered as an overlapping array of small dipoles. Therefore, if the dipole is divided into N segments, we can consider that there are $(N-1)$ overlapping small dipoles. The expansion function for the mth element is given by [24]

$$\begin{aligned} \overline{F}_m(z) &= \hat{z}\frac{\sin\beta(z-z_{m1})}{\sin(\beta\Delta)}, \quad z_{m1} \le z \le z_{m2}\ , \\ \overline{F}_m(z) &= \hat{z}\frac{\sin\beta(z_{m3}-z)}{\sin(\beta\Delta)}, \quad z_{m2} \le z \le z_{m3}\ , \end{aligned} \tag{1}$$

where Δ is the segment length. The electric field for the mth element is given by [24]

$$\begin{aligned} E_{zm} = -j30\Bigg[&\frac{e^{-j\beta R_{m1}}}{R_{m1}\sin\beta(z_{m2}-z_{m1})} \\ &- \frac{e^{-j\beta R_{m2}}\sin\beta(z_{m3}-z_{m1})}{R_{m2}\sin\beta(z_{m2}-z_{m1})\sin\beta(z_{m3}-z_{m2})} \\ &+ \frac{e^{-j\beta R_{m3}}}{R_{m3}\sin\beta(z_{m3}-z_{m2})}\Bigg], \end{aligned} \tag{2}$$

where $R_{m1} = \sqrt{\rho^2+(z-z_{m1})^2}$, $R_{m2} = \sqrt{\rho^2+(z-z_{m2})^2}$, and $R_{m3} = \sqrt{\rho^2+(z-z_{m3})^2}$. The generalized impedance matrix for a dipole can be computed from

$$\begin{aligned} Z_m = -\Bigg[\int_{z_{n1}}^{z_{n2}} &\frac{\sin\beta(z-z_{n1})}{\sin(\beta\Delta)} + \int_{z_{n2}}^{z_{n3}} \frac{\sin\beta(z_{n3}-z)}{\sin(\beta\Delta)}\Bigg]\frac{j30}{\sin(\beta\Delta)} \\ &\times\left[\frac{e^{-j\beta R_{m1}}}{R_{m1}} - 2\cos(\beta\Delta)\frac{e^{-j\beta R_{m2}}}{R_{m2}} + \frac{e^{-j\beta R_{m3}}}{R_{m3}}\right]dz. \end{aligned} \tag{3}$$

The impedance matrix must be modified to take into account for the dielectric and magnetic loading. According to [23], the additional matrix element for a z directed dipole due to dielectric loading is given by

$$\Delta Z_{mn\_\varepsilon} = -\frac{P}{2\,\pi\,j\,\omega\,\varepsilon_0}\int_{m,n} F_m'(z)F_n'(z)dz, \tag{4}$$

where (m, n) denote the region of z shared by dipoles m and n, ω is the angular frequency, and ε_0 is the free space permittivity ($\varepsilon_0 = 8.85\times10^{-12}$ F/m). $F_m\prime(z)$ and $F_n\prime(z)$ are the derivatives of the expansion function of the mth and nth elements, respectively. The dimensionless parameter P is given by

$$P = \int_a^b \frac{\varepsilon_{r2}-\varepsilon_{r1}}{\varepsilon_{r2}\,\rho}d\rho = \frac{(\varepsilon_{r2}-\varepsilon_{r1})}{\varepsilon_{r2}}\ln\left(\frac{b}{a}\right), \tag{5}$$

where $\varepsilon_{r1} = 1$ is the relative permittivity of air and ε_{r2} is the relative permittivity of the loading DNG or DPS medium and $\Delta Z_{mn\_\varepsilon}$ is zero if dipoles m and n do not share a segment. Therefore, to observe the effect of $\Delta Z_{mn\_\varepsilon}$ only the currents on the adjacent two segments are considered. A similar procedure is followed to take into account of the magnetic loading effect. This can be computed by [25]

$$\Delta Z_{mn\_\mu} = Q\times\frac{j\omega\mu_0}{2\pi}\int_{m,n} F_m'(z)F_n'(z)dz, \tag{6}$$

where μ_0 is the free space permeability ($\mu_0 = 4\pi\times10^{-7}$ H/m) and the dimensionless parameter Q is given by

$$Q = \int_a^b \frac{\mu_r-1}{\rho}d\rho = (\mu_r-1)\ln\left(\frac{b}{a}\right), \tag{7}$$

where μ_r is the relative permeability of the loading DNG or DPS medium. The first row of the modified impedance matrix can be computed as

$$Z_{m1} = Z_m + \Delta Z_{mn\_\varepsilon} + \Delta Z_{mn\_\mu}. \tag{8}$$

The built-in Toeplitz algorithm in Matlab was used to generate the complete square impedance matrix Z_{mn}. A delta gap excitation with a 1 V source was considered at the center of the dipole. The current distribution on the antenna was computed using the following $[Z_{mn}]\,[I] = [V]$. The input impedance and radiation pattern were then computed from the current distribution.

3. PRELIMINARY RESULTS

To validate the formulation described above a dipole antenna loaded with a thin layer of dielectric material was considered. The parameters of this antenna were the same as given in [23]: length, $L = 8$ inch, diameter, $2a = 0.025$ inch, loading diameter, $2b = 0.146$ inch, $\varepsilon_r = 2.3$, and $\mu_r = 1$. Table 1 compares our results (computed admittance) with those given in [23]. At all frequencies the resistance and reactance values obtained are in good agreement. Increasing the number of elements decreases the segment size (Δ) which has the potential to improve computational accuracy. However, a very small Δ with respect to the wavelength can cause oscillations and in general, a large segment size to wire radius ratio (Δ/r) is needed to ensure high accuracy. Based on these consideration, we used $N = 10$ for all analyses in this paper.

4. EFFECTS OF PARAMETERS P AND Q

Both dielectric and magnetic loadings affect the current distributions of a dipole antenna. This can be understood by examining the parameters P and Q defined in (5) and (7).

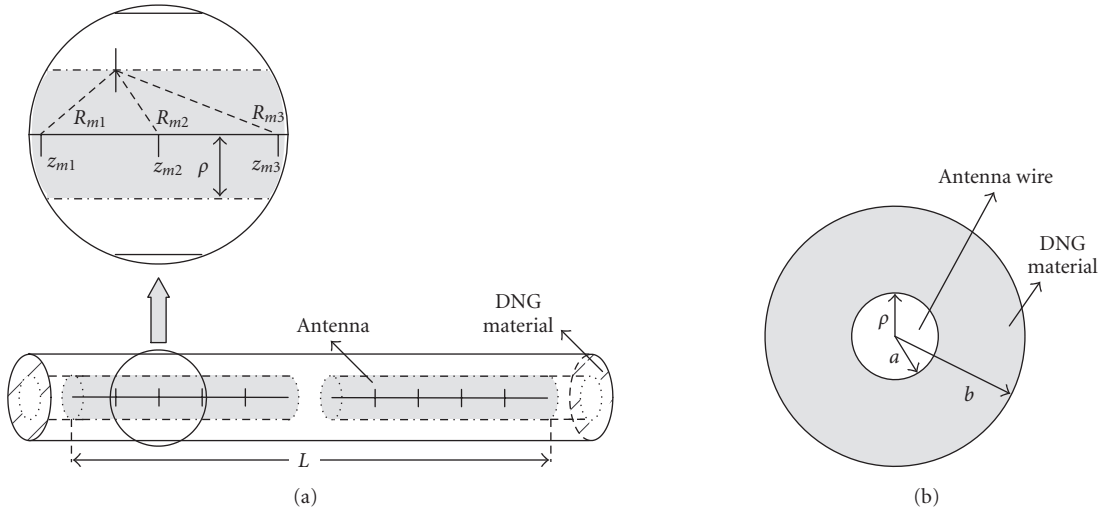

Figure 1: (a) Dipole antenna loaded with a DNG material; (b) cross-sectional view.

Table 1: Comparison of our results with literature data.

Frequency (MHz)	Admittance [23]	Admittance [Our results]
450	$0.3 + j3.7$	$0.3 + j3.9$
600	$9.5 + j10.5$	$12.7 + j9.6$
750	$2.8 - j4.2$	$2.6 - j3.9$
1050	$0.7 - j0.3$	$0.696 - j0.33$

Note that if P and Q attain values other than zero (this is the case for DPS with $\varepsilon_r, \mu_r \neq 1$ or DNG loading) they add with the existing terms in the generalized impedance matrix of the dipole (see (8)) and hence change the current distribution on the antenna. Once the radii of the inner and outer shells are fixed, P and Q depend only on ε_r and μ_r (see (5) and (7)). Consider a conventional DPS medium. If $\varepsilon_r = \mu_r = 1$, $P = Q = 0$. Increasing ε_r increases P, which attains its maximum value $1 \times \ln(b/a)$ when $\varepsilon_r \to \infty$. Similarly, Q also increases as μ_r increases. Increase in either P or Q increases the antenna electrical length, the peak input admittance, and narrows the bandwidth [26].

From (5) and (7) it is clear that P is positive for both DPS with $\varepsilon_r, \mu_r > 1$ and DNG materials whereas Q is positive for DPS with $\varepsilon_r, \mu_r > 1$ and negative for DNG materials. The effect of ε_r and μ_r on P and Q for both DPS and DNG materials are shown in Figure 2. For DPS materials, no results are shown when $0 < (\varepsilon_r, \mu_r) < 1$ as because no such material exists.

The parameter P attains its maximum value $1 \times \ln(b/a)$ for a DPS medium which is the lowest possible value for a DNG medium. In contrast, Q attains positive values for DPS media and negative values for DNG media. Thus with DNG loading P tends to make the antenna electrically longer while Q tends to make it shorter. To understand the cumulative effect of P and Q in a DNG medium, the combination of ε_r, μ_r may be distinctly divided into two classes: case I $(-1 < (\varepsilon_r, \mu_r) < 0)$ and case II $(-\infty \leq (\varepsilon_r, \mu_r) < -1)$. For case I, P is larger than Q, and for case II, Q is larger than P.

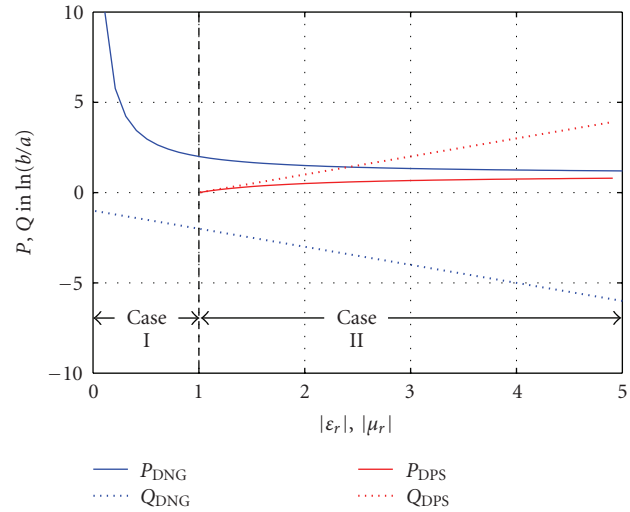

Figure 2: Effect of ε_r and μ_r on parameter P and Q for both DPS and DNG material.

The smaller the $|\varepsilon_r|$, the higher is the P and the higher is the $|\Delta Z_{mn\text{-}\varepsilon}|$ (see (4)). On the other hand, the smaller the $|\mu_r|$, the smaller is the $|Q|$ and the smaller is the $|\Delta Z_{mn\text{-}\mu}|$ (see(6)). Hence, for case I, the impedance matrix (8) is more affected by P than Q. For case II, P and Q vary as $1 < P < 2$ and $-\infty < Q < -2$, respectively. Hence, the impedance matrix is affected more by Q than P for case II.

5. RESULTS

A dipole antenna loaded with a cylindrical shell of homogeneous material (either double negative—DNG—or double positive—DPS) as illustrated in Figure 1 is considered. The length of the antenna, L is taken to be 200 mm, which is $0.5\,\lambda$ (λ is the wavelength in free space) at 750 MHz. The wire radius ρ is 0.3175 mm. The DNG material surrounding the antenna has an inner radius of $a = 0.3175$ mm and an outer

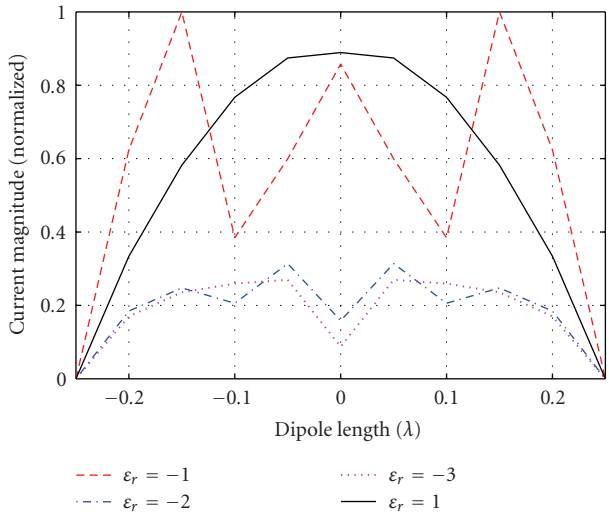

Figure 3: Computed current distribution at 750 MHz. Other parameters: $L = 200$ mm, $r = 0.3175$ mm, $a = 0.3175$ mm, $b = 1.8542$ mm, $\mu_r = 1$, and $N = 10$.

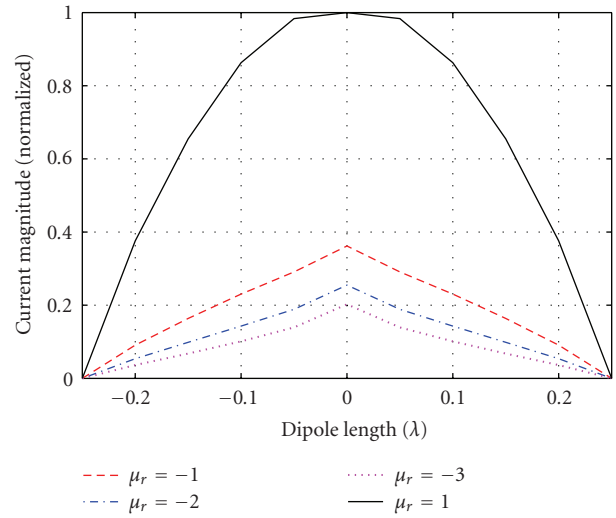

Figure 4: Current distribution at 750 MHz. Other parameters: $L = 200$ mm, $r = 0.3175$ mm, $a = 0.3175$ mm, $b = 1.8542$ mm, $\varepsilon_r = 1$, and $N = 10$.

radius of $b = 1.8542$ mm. Since $a = \rho$, there is no air gap between the antenna and the loading medium. The relationship between the permittivity (ε_r) and permeability (μ_r) of a double negative material is given by [4] $\varepsilon_r \approx \mu_r + j(2S_{11}/k_0 d)$. This expression shows that when $S_{11} \to 0$, which is the case for a DNG material, ε_r and μ_r should exhibit very similar responses. This is the reason we used same values for ε_r and μ_r in our study. The effect of DNG material loading on the current distribution of the antenna can be easily computed using the moment method formulation described in Section 2. Once the current distribution is known, other antenna characteristics, such as the input impedance and radiation pattern, can be also be calculated there from.

5.1. Effect of negative permittivity on current distribution

The effect of negative relative permittivity ε_r ($\mu_r = 1$, hence $Q = 0$) on the current distribution of a $0.5\,\lambda$ dipole antenna is shown in Figure 3. Similarly, the current distribution of a half wavelength dipole in free space ($\varepsilon_r = \mu_r = 1$) is also shown in Figure 3 for comparison. Unlike the current distribution for the antenna in free space, the current maximum for the antenna in the medium with negative relative permittivity shifts away from the center of the dipole. It is also clear from Figure 3 that for cases with $\varepsilon_r = -2$ and $\varepsilon_r = -3$ the current distributions exhibit two maximas occurring away from the center of the antenna while they show the presence of current minimas at the antenna center. These characteristics are representative of an electrically long dipole. Interestingly, for $\varepsilon_r = -1.0$, three current maximas are observed. Comparing the current distributions for $\varepsilon_r = -3$ and $\varepsilon_r = -2$, the difference observed is very minor. In contrast, significant difference is observed between the current distributions for $\varepsilon_r = -2$ and $\varepsilon_r = -1$. This is primarily due to the fact that the change in the parameter P is small when ε_r changes from

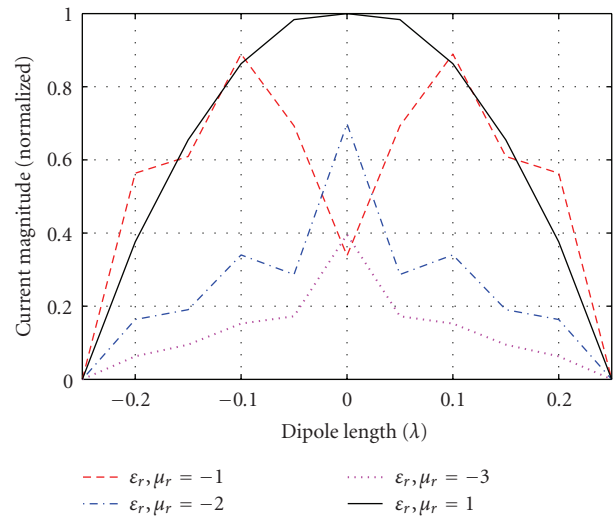

Figure 5: Current distributions at 750 MHz with ε_r and μ_r as parameters. Other parameters: $L = 200$ mm, $a = 0.3175$ mm, $b = 1.8542$ mm, $r = 0.3175$ mm, and $N = 10$.

-3 to -2 while it is large when it changes from -2 to -1 (see Figure 2). The large change in P changes the impedance matrix more significantly which results in appreciable difference in the current distribution.

5.2. Effect of negative permeability on current distribution

The current distributions of a dipole antenna loaded with a homogeneous medium with negative relative permeability μ_r($\varepsilon_r = 1$, hence $P = 0$) are shown in Figure 4. The current distributions are triangular which resemble the current distribution of a short dipole ($l < \lambda/10$). From Figure 2, Q

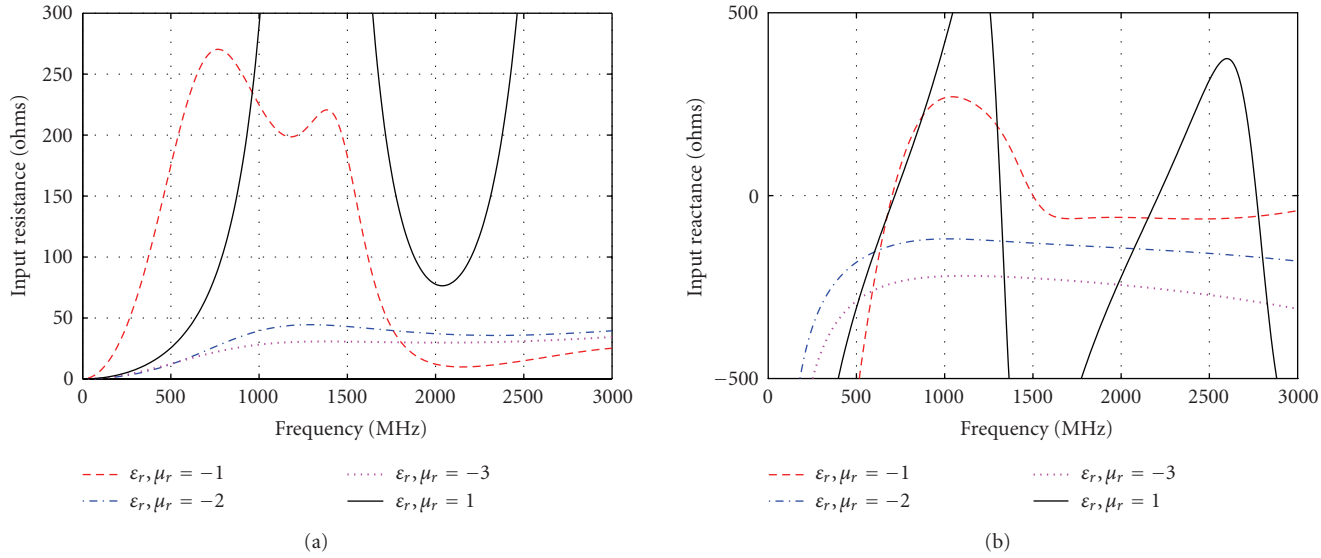

FIGURE 6: (a) Input resistance, and (b) reactance. Other parameters: $L = 200$ mm, $a = 0.3175$ mm, $b = 1.8542$ mm, $r = 0.3175$ mm, and $N = 10$.

decreases linearly as $|\mu_r|$ increases, this in turn decreases the antenna electrical length. A gradual change in current magnitude is observed as μ_r is varied. The higher the $|\mu_r|$ value, the lower is the peak current magnitude.

5.3. *Effects of negative permittivity and permeability on current distribution*

The change in current distribution due to the combined effects of P and Q for various DNG parameters is presented in Figure 5. As mentioned, with DNG loading P tends to increase and Q tends to decrease the antenna electrical length. However, when the absolute values of P and Q are the same, it does not necessarily mean that their effect on the impedance matrices as defined by (4) and (6) will be the same. As apparent, when $\varepsilon_r = \mu_r = -1$ the current peak shifts from the center indicating the behavior of an electrically long antenna. As $|\varepsilon_r|$ and $|\mu_r|$ increases significantly the parameter Q plays a more dominant role than P. The results of which are manifested in triangular type current distributions as shown in Figure 5.

5.4. *Input impedance*

Based on the current distribution and the delta-gap voltage source, input impedance of the dipole shown in Figure 1 was computed from 100 MHz to 3000 MHz. The dipole wire radius, $\rho = 0.3175$ mm and the shell inner and outer radii were $a = 0.3175$ and $b = 1.8542$ mm, respectively. Figure 6 illustrates the variation of input resistance and reactance with frequency for various negative relative permittivity and permeability values as parameters. Free space ($\varepsilon_r = \mu_r = 1$) data for the dipole antenna are also presented in the same figure for comparison. The antenna in free space resonates around 750 MHz. The resistance and reactance characteristics in free space are strikingly different from those in the DNG medium. The input resistance and reactance for this case reflect the characteristics of a conventional thin-wire dipole which exhibits multiple series and parallel type resonances [26]. The variation of the input resistance and reactance with frequency is quite pronounced. Thus, the potential for wideband operation is limited. By contrast, for $\varepsilon_r = \mu_r = -2$, the input reactance characteristics exhibit nearly zero slope with frequency. This indicates that the reactance is almost independent of frequency for the frequency range over which it has a zero slope. Interestingly, the input resistance data for this case are nearly 50 Ω from 100 to 3000 MHz. These characteristics are unique and different from those observed with conventional dipoles whether in free space or covered with a homogeneous dielectric shell. For $\varepsilon_r = \mu_r = -2$ and $\varepsilon_r = \mu_r = -3$, the antenna does not exhibit resonant behavior. However, as we changed both ε_r and μ_r from -3 to -2 to -1, the reactance curve progressively moved closer to the zero reactance line (see Figure 6(b)) within 1500 to 3000 MHz. Thus, if it is possible to design a DNG material which will provide the resistance characteristics shown in Figure 6(a) for $\varepsilon_r = \mu_r = -2$ and at the same time bring the reactance values close to zero, a multioctave broadband antenna will result. Comparing the three pairs of DNG values, it is clear that an optimum DNG medium with optimum ε_r, μ_r, a, and b will be required to achieve good performance.

Further studies were conducted by considering more gradual variation in ε_r, μ_r from -1 to -1.2. Input resistance and reactance data for $\varepsilon_r = \mu_r = 1, -1.1$, and -1.2 are shown in Figures 7(a) and 7(b). It is clear that the high Q resonance characteristics (given by the rapid impedance change with frequency) are not exhibited by the antenna when it is covered with a DNG medium. Considering a feed transmission line with a characteristic impedance of 200 Ω antenna, VSWR was computed (shown in Figure 7(c)). For $\varepsilon_r = \mu_r = -1.1$ the VSWR bandwidth (within 2 : 1) is 92%.

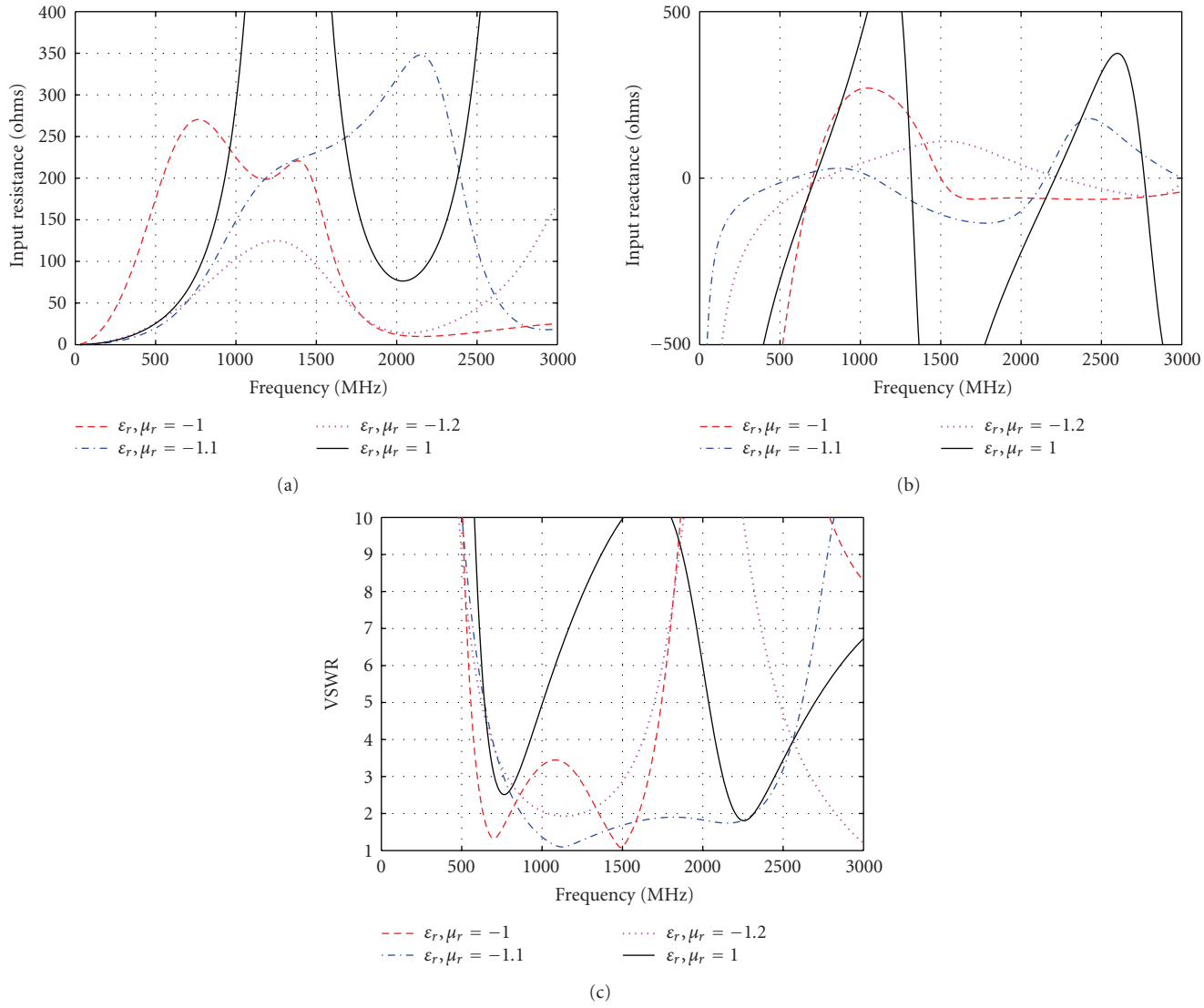

Figure 7: (a) Input resistance; (b) reactance, and (c) VSWR. Other parameters: $L = 200$ mm, $a = 0.3175$ mm, $b = 1.8542$ mm, $r = 0.3175$ mm, and $N = 10$.

5.5. Radiation characteristics

Computed normalized radiation patterns at 750, 1500, 1875, and 2250 MHz are shown in Figure 8. The radiation pattern for the antenna in free space is also shown for comparison. Due to ϕ symmetry, patterns are plotted in the elevation plane only. The beam width of the antenna in free space is 70° and 46° at 750 and 1500 MHz, respectively. In contrast, the beam width of the antenna in the DNG medium is 70° and 60° at those frequencies. Further increase in antenna electrical length decreases the beamwidth of the antenna in free-space as exhibited by Figures 8(c) and 8(d). The antenna also shows multiple lobes and at 2250 MHz the principal direction of radiation shifts from ±90° to ±40° and ±110°. Interestingly, these characteristics are not observed when the antenna is covered with a DNG medium. As the frequency increases from 750 MHz to 2250 MHz, the antenna pattern retains its original Figure 8 shape. The beamwidth decreases and then increases. To understand the beam broadening at 1875 MHz and more so at 2250 MHz we need to look at the effects of the antenna electrical length and the DNG loading on the radiation pattern. For a conventional dipole in free-space as the antenna length increases to 1.5λ, the pattern becomes butterfly shaped with the direction of the main beam being shifted. By contrast, the DNG loading has a tendency to focus the radiation towards $\theta = 90°$. These two forces when acting together result in the pattern shown using the dashed line in Figure 8(d). The pattern main beam direction is along $\theta = 90°$ and the beam is broader because of the lobing effect due to the loner antenna electrical length.

5.6. Resonance at a lower frequency

Electrically small dipole antennas are greatly desired for many wireless applications. Their usage is inhibited due to

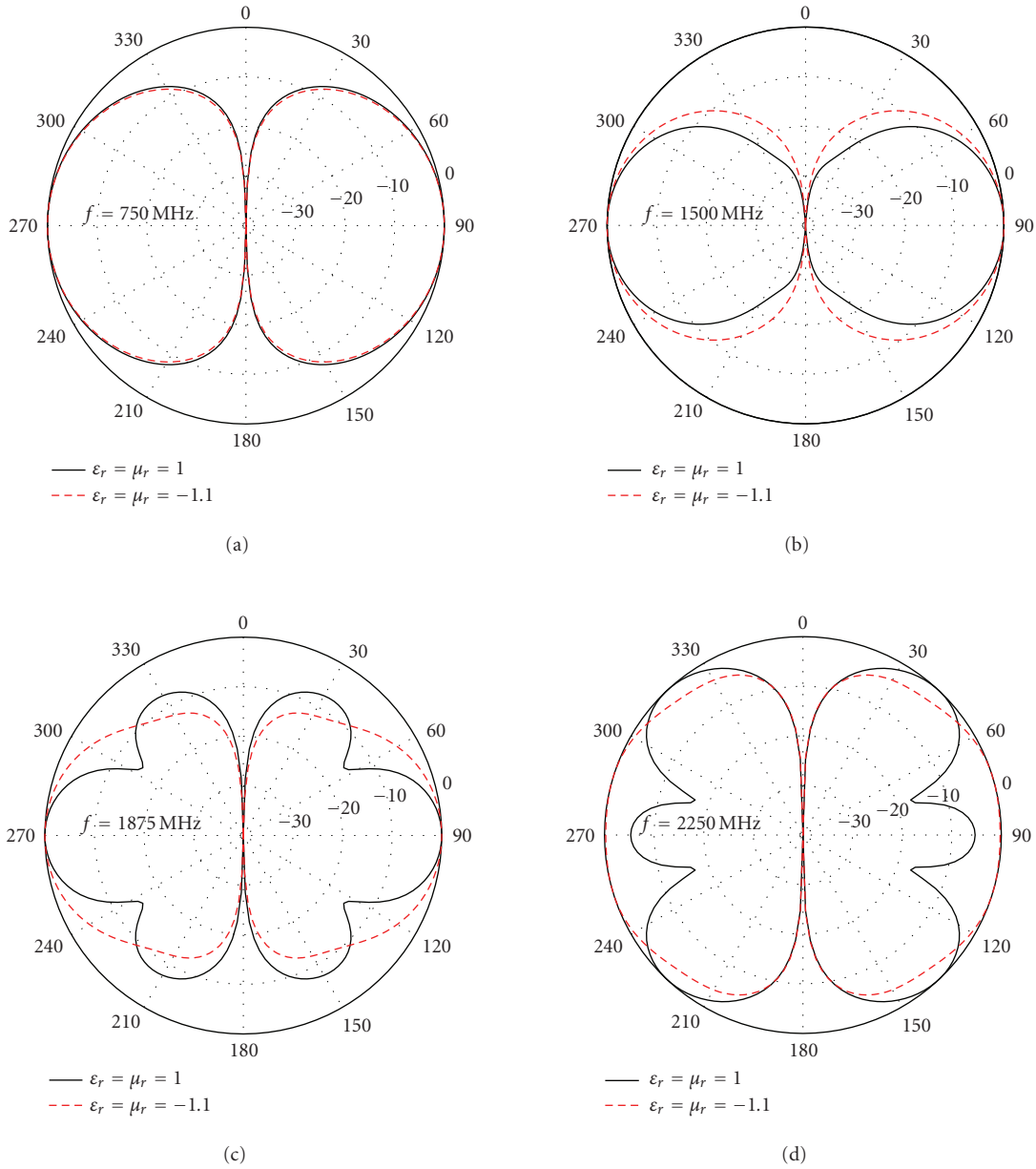

Figure 8: Normalized elevation plane patterns at (a) 750 MHz, (b) 1500 MHz, (c) 1875 MHz, and (d) 2250 MHz. Other parameters: $L = 200$ mm, $a = 0.3175$ mm, $b = 1.8542$ mm, $r = 0.3175$ mm, and $N = 10$.

their relatively large capacitive reactance and small input resistance [26]. Even though the reactance can be nullified by adding a series inductance and the input resistance can be matched using a transformer, the resulting antenna is extremely inefficient. The loss in efficiency results from the antenna loss resistance and the ohmic losses in the matching circuit. Thus, it is always desirable to design antennas that are self-resonant. Some examples of small self-resonant antennas are the normal mode helical, the meander and the zigzag antenna [27–29]. Many of these antennas are widely used in present day mobile phones and wireless radios. However, using these structures useful antenna design can be achieved up to a size reduction of approximately 50 percent. For instance, consider an 80 mm long mobile phone whip antenna at 900 MHz which can be reduced to approximately 30 mm using a helical or meander geometry. We wanted to explore the possibility of designing miniature self-resonant antennas using a cylindrical shell of DNG material as the cover for a dipole.

We have observed before that increasing P increases the electrical length of the antenna. Maximum increase in P occurs when $-1 < \varepsilon_r, \mu_r < 0$. Thus, to design electrically small dipole antennas loaded with a cylindrical shell of DNG medium, we should have ε_r and μ_r values that fall in this range. The effect of varying ε_r, μ_r from -0.7 to -0.5 is shown in Figure 9. It is clear that decreasing $|\varepsilon_r|$, $|\mu_r|$ results in the

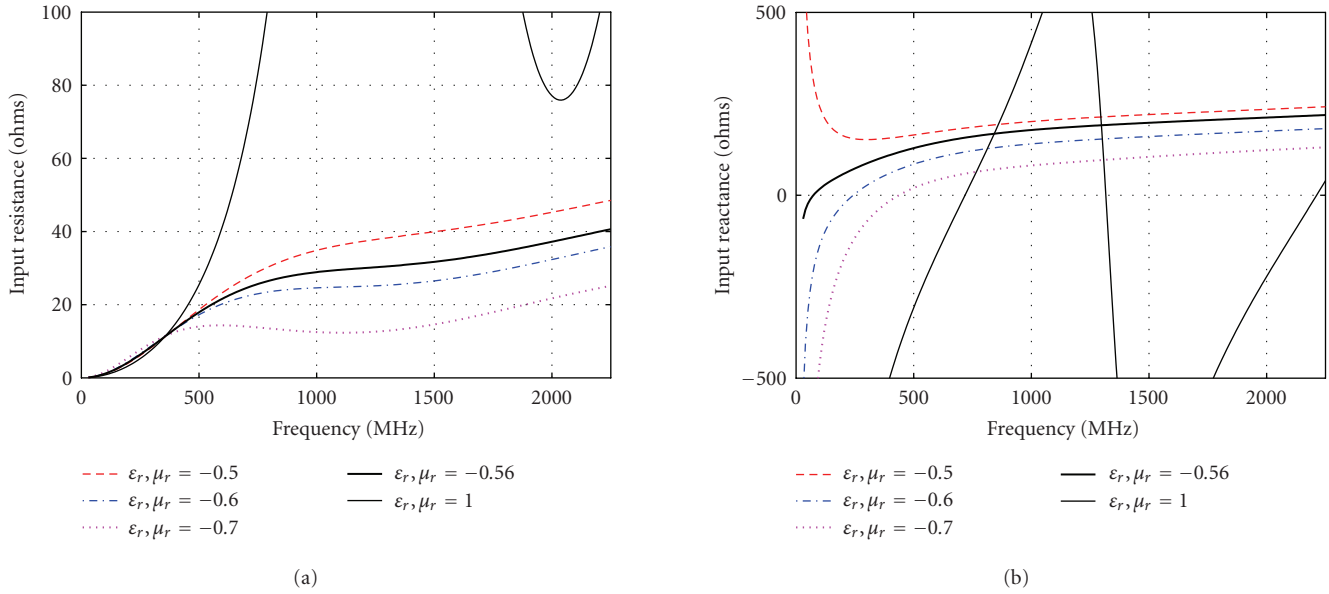

Figure 9: Resonance at lower frequencies: (a) input resistance and (b) reactance. Other parameters: $L = 200\,\text{mm}$, $a = 0.3175\,\text{mm}$, $b = 1.8542\,\text{mm}$, $r = 0.3175, \text{mm}\ N = 10$.

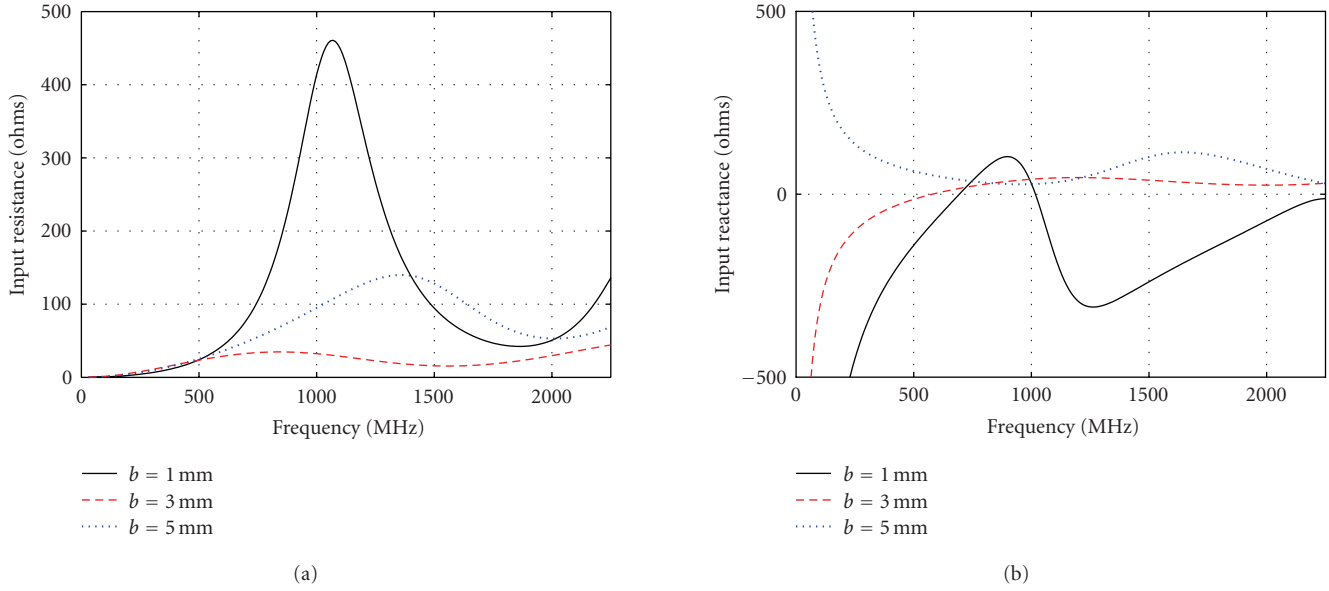

Figure 10: Effect of DNG shell thickness b on antenna input impedance. Other parameters: $L = 200\,\text{mm}$, $a = 0.3175\,\text{mm}$, $r = 0.3175\,\text{mm}$, $\varepsilon_r = \mu_r = -1$, and $N = 10$.

input reactance being less capacitive. For $\varepsilon_r, \mu_r = -0.5$, the antenna reactance is entirely inductive. For $\varepsilon_r, \mu_r = -0.6$ the dipole shows resonance at 250 MHz. It appears that by varying ε_r, μ_r within -0.5 to -0.6 it is possible to achieve resonance at a lower frequency. The dipole shows resonance at 100 MHz ($l = \lambda/15$) for $\varepsilon_r = \mu_r = -0.56$. The input resistance is unchanged compared to its free space counterpart (see Figure 9(a)). The radiation patterns for the electrically small dipole for $\varepsilon_r = \mu_r = -0.56$ showed no significant change.

5.7. *Influence of inner and outer shell radii on input impedance*

Input impedance data as function of frequency with the outer shell radius, b as the parameter are shown in Figure 10. Other parameters were $a = 0.3175\,\text{mm}$ and $\varepsilon_r = \mu_r = -1$. For smaller shell thickness ($b = 1\,\text{mm}$), antenna impedance resemble that of a dipole antenna in free space. As the shell thickness increases ($b = 3$ and $5\,\text{mm}$), DNG behavior dominates which is exhibited by flatter reactance and resistance

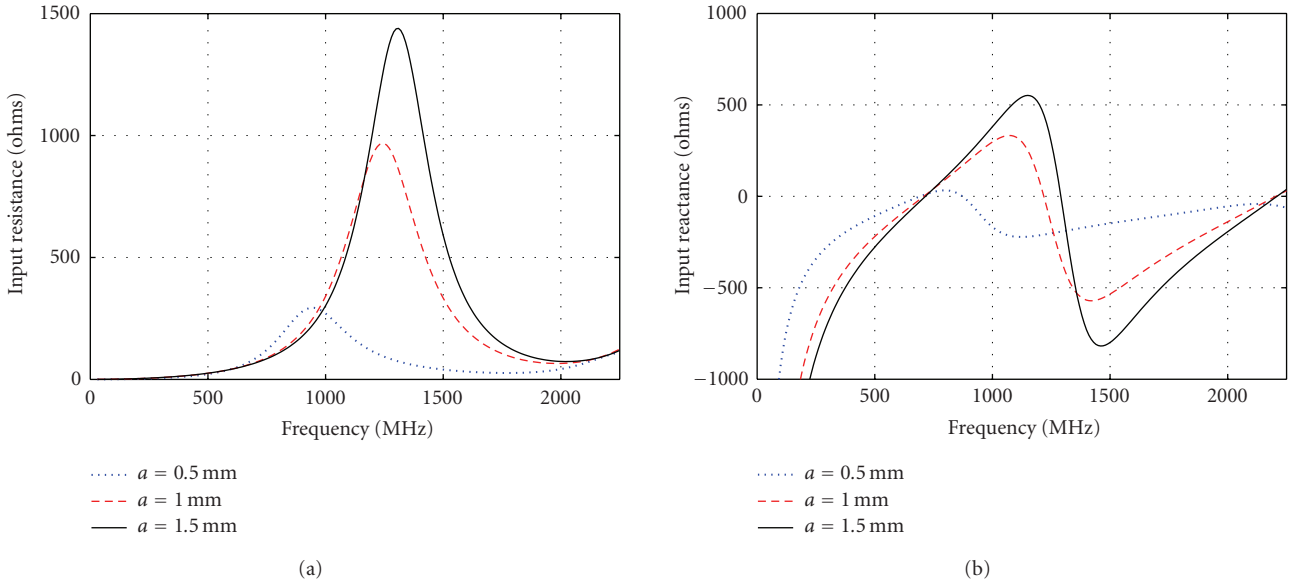

FIGURE 11: Effect of inner shell radius a on antenna input impedance. Other parameters: $L = 200$ mm, $b = 1.8542$ mm, $r = 0.3175$ mm, $\varepsilon_r = \mu_r = -1$, and $N = 10$.

characteristics. The shell thickness b also affects the resonance property of the antenna, antenna reactance becomes less capacitive as b increases from 1 to 3 mm, finally becoming inductive when $b = 5$ mm.

Increasing the inner radius (a) of the DNG shell while keeping b fixed decreases the effective thickness of the DNG medium and the antenna characteristics approach that of its free space counterpart (see Figure 11).

6. CONCLUSION

The characteristic of a wire dipole antenna loaded with a cylindrical shell of DNG material was studied. The piecewise sinusoidal Galerkin moment method was used to study the behavior of the antenna system. It was observed that the effect of loading the dipole antenna with a DNG medium is primarily governed by the two dimensionless parameters, P and Q, which in turn depend on the relative permittivity, permeability, and the ratio of the outer and inner radii of the loading cylindrical medium. However, for a dipole antenna loaded with a DNG material, P is always larger and Q is always smaller compared to the P and Q values when the antenna is loaded with a DPS material. Any changes in these parameters change the current distribution of the antenna which changes the antenna characteristics. Therefore, for an antenna loaded with a DNG material, whether P or Q dominates is significant. Simply stating, a decrease in Q is more significant than an increase in P when $(\varepsilon_r, \mu_r) < -1$. Within this range of values, we have demonstrated that broadband antennas can be designed. For $\varepsilon_r = \mu_r = -1.1$ we have shown that 92% bandwidth can be achieved within 2 : 1 VSWR.

In contrast, for $-1 < (\varepsilon_r, \mu_r) < 0$, P dominates over Q. Within these ranges of values one may design electrically small antennas. We have shown an example of a $\lambda/15$ dipole loaded with a medium with $\varepsilon_r = \mu_r = -0.56$. We have found that the radiation patterns of the antenna in a DNG medium do not show any changes in the direction of the principal beam as the antenna electrical length increases. No side lobes were observed for antennas that were as long as 1.5λ.

The formulation presented in this paper is valid for a cylindrical shell with small thickness with respect to the wavelength. Major implementation challenges that remain to be explored include (1) the experimental fabrication of a DNG medium in the form of a cylindrical shell, (2) the homogeneous nature of the medium fabricated, and (3) the development of materials for which the negative relative permittivity and permeability are frequency independent.

ACKNOWLEDGMENT

This work was supported in part by the National Science Foundation (NSF) Career Award ECS-0237783.

REFERENCES

[1] V. G. Veselago, "The electrodynamics of substances with simultaneously negative values of ϵ and μ," *Soviet Physics Uspekhi*, vol. 10, no. 4, pp. 509–514, 1968.

[2] J. B. Pendry, A. J. Holden, D. J. Robbins, and W. J. Stewart, "Magnetism from conductors and enhanced nonlinear phenomena," *IEEE Transactions on Microwave Theory and Techniques*, vol. 47, no. 11, pp. 2075–2084, 1999.

[3] N. Engheta, S. R. Nelatury, and A. Hoorfar, "The role of geometry of inclusions in forming metamaterials with negative permittivity and permeability," in *Proceedings of the 27th General Assembly of International Union of Radio Science (URSI GA '02)*, Maastricht, The Netherlands, August 2002.

[4] R. W. Ziolkowski, "Design, fabrication, and testing of double negative metamaterials," *IEEE Transactions on Antennas and Propagation*, vol. 51, no. 7, pp. 1516–1529, 2003.

[5] R. Marqués, F. Mesa, J. Martel, and F. Medina, "Comparative analysis of edge- and broadside- coupled split ring resonators for metamaterial design—theory and experiments," *IEEE Transactions on Antennas and Propagation*, vol. 51, no. 10, part 1, pp. 2572–2581, 2003.

[6] S. A. Tretyakov, S. Maslovski, and P. A. Belov, "An analytical model of metamaterials based on loaded wire dipoles," *IEEE Transactions on Antennas and Propagation*, vol. 51, no. 10, part 1, pp. 2652–2658, 2003.

[7] L. X. Ran, J. Huangfu, H. Chen, et al., "Experimental study on several left-handed metamaterials," *Progress in Electromagnetic Research*, vol. 51, pp. 249–279, 2005.

[8] A. Sanada, C. Caloz, and T. Itoh, "Planar distributed structures with negative refractive index," *IEEE Transactions on Microwave Theory and Techniques*, vol. 52, no. 4, pp. 1252–1263, 2004.

[9] G. V. Eleftheriades, A. K. Iyer, and P. C. Kremer, "Planar negative refractive index media using periodically L-C loaded transmission lines," *IEEE Transactions on Microwave Theory and Techniques*, vol. 50, no. 12, pp. 2702–2712, 2002.

[10] J. B. Pendry, "Negative refraction makes a perfect lens," *Physical Review Letters*, vol. 85, no. 18, pp. 3966–3969, 2000.

[11] K. Li, S. J. McLean, R. B. Greegor, C. G. Parazzoli, and M. H. Tanielian, "Free-space focused-beam characterization of left-handed materials," *Applied Physics Letters*, vol. 82, no. 15, pp. 2535–2537, 2003.

[12] A. Alù and N. Engheta, "Pairing an epsilon-negative slab with a mu-negative slab: resonance, tunneling and transparency," *IEEE Transactions on Antennas and Propagation*, vol. 51, no. 10, part 1, pp. 2558–2571, 2003.

[13] E. Ozbay, K. Aydin, E. Cubukcu, and M. Bayindir, "Transmission and reflection properties of composite double negative metamaterials in free space," *IEEE Transactions on Antennas and Propagation*, vol. 51, no. 10, part 1, pp. 2592–2595, 2003.

[14] H. Okabe, C. Caloz, and T. Itoh, "A compact enhanced-bandwidth hybrid ring using an artificial lumped-element left-handed transmission-line section," *IEEE Transactions on Microwave Theory and Techniques*, vol. 52, no. 3, pp. 798–804, 2004.

[15] I.-H. Lin, M. DeVincentis, C. Caloz, and T. Itoh, "Arbitrary dual-band components using composite right/left-handed transmission lines," *IEEE Transactions on Microwave Theory and Techniques*, vol. 52, no. 4, pp. 1142–1149, 2004.

[16] M. A. Antoniades and G. V. Eleftheriades, "Compact linear lead/lag metamaterial phase shifters for broadband applications," *IEEE Antennas and Wireless Propagation Letters*, vol. 2, no. 1, pp. 103–106, 2003.

[17] S. N. Burokur, M. Latrach, and S. Toutain, "Theoretical investigation of a circular patch antenna in the presence of a left-handed medium," *IEEE Antennas and Wireless Propagation Letters*, vol. 4, no. 1, pp. 183–186, 2005.

[18] B.-I. Wu, W. Wang, J. Pacheco, X. Chen, T. M. Grzegorczyk, and J. A. Kong, "A study of using metamaterials as antenna substrate to enhance gain," *Progress In Electromagnetics Research*, vol. 51, pp. 295–328, 2005.

[19] R. W. Ziolkowski and A. D. Kipple, "Application of double negative materials to increase the power radiated by electrically small antennas," *IEEE Transactions on Antennas and Propagation*, vol. 51, no. 10, part 1, pp. 2626–2640, 2003.

[20] A. Erentok and R. W. Ziolkowski, "Dipole antennas enclosed in double negative (DNG) and single-negative (SNG) nested spheres: efficient electrically small antennas," in *Proceedings of the IEEE Antennas and Propagation Society International Symposium*, vol. 1B, pp. 252–255, Washington, DC, USA, July 2005.

[21] R. W. Ziolkowski, "Applications of metamaterials to realize efficient electrically small antennas," in *Proceedings of the IEEE International Workshop on Antenna Technology: Small Antennas and Novel Metamaterials (IWAT '05)*, pp. 7–10, Singapore, March 2005.

[22] K. M. Z. Shams and M. Ali, "The input impedance of a dipole antenna loaded by a cylindrical shell of double negative (DNG) meta-material," in *Proceedings of the IEEE Antennas and Propagation Society International Symposium and URSI/USNC Meeting*, Washington, DC, USA, July 2005.

[23] J. H. Richmond and E. H. Newman, "Dielectric coated wire antennas," *Radio Science*, vol. 11, no. 1, pp. 13–20, 1976.

[24] W. L. Stutzman and G. A. Thiele, *Antenna Theory and Design*, John Wiley & Sons, New York, NY, USA, 1981.

[25] J. P. Y. Lee and K. G. Balmain, "Wire antennas coated with magnetically and electrically lossy material," *Radio Science*, vol. 14, no. 3, pp. 437–445, 1979.

[26] C. A. Balanis, *Antenna Theory*, John Wiley & Sons, New York, NY, USA, 2nd edition, 1997.

[27] M. Ali, S. S. Stuchly, and K. Caputa, "Characteristics of bent wire antennas," *Journal of Electromagnetic Waves and Applications*, vol. 9, no. 9, pp. 1149–1162, 1995.

[28] M. Ali, M. Okoniewski, and S. S. Stuchly, "Study of a printed meander antenna using the FDTD method," *Microwave and Optical Technology Letters*, vol. 37, no. 6, pp. 440–444, 2003.

[29] J. T. Rowley, R. B. Waterhouse, and K. H. Joyner, "Modeling of normal-mode helical antennas at 900 MHz and 1.8 GHz for mobile communications handsets using the FDTD technique," *IEEE Transactions on Antennas and Propagation*, vol. 50, no. 6, pp. 812–820, 2002.

AUTHOR CONTACT INFORMATION

Khan M. Z. Shams: Department of Electrical Engineering, University of South Carolina, Swearingen Engineering Center, SC 29208, Colombia; shams@engr.sc.edu

Mohammod Ali: Department of Electrical Engineering, University of South Carolina, Swearingen Engineering Center, SC 29208, Colombia; alimo@engr.sc.edu